A&A 417, 411–419 (2004)
DOI: 10.1051/0004-6361:20031085

Astronomy & Astrophysics

BVRI surface photometry of mixed morphology pairs of galaxies

II. The second data set⋆,⋆⋆

A. Franco-Balderas[1], H. M. Hernández-Toledo[1], and D. Dultzin-Hacyan[1]

Instituto de Astronomía – UNAM – Apartado Postal 70-264, CP 04510 México DF, México
e-mail: [hector;deborah]@astroscu.unam.mx

Received 10 April 2003 / Accepted 22 October 2003

Abstract. In order to analyze the photometric signature of gravitational interactions in spiral and elliptical galaxies, we present results of multicolor broad band (*BVRI*) surface photometry for a second set of 10 mixed pairs drawn from the Karachentsev Catalogue of Isolated Pairs of Galaxies (KPG). We report total magnitudes and colors, as well as surface brightness, color and geometric (ϵ, PA and a_4/a) profiles. Most of this subsample have photometric parameters homogeneously derived for the first time. Internal and external data comparisons show consistency within the estimated errors. We find 1 true (E+S) pair and 4 probable (E+S) pairs ((E/S0+S) cases) in the present sample. The remaining objects include 3 lenticular-spiral (S0+S) systems, 1 spiral-spiral (S+S) pair and 1 probable spiral-spiral pair ((S0/Sa+S) case). Four lenticular galaxies show evidence of underlying (perhaps induced) structures like bars/arms. Among the spiral components, an over-representation of early (Sa−Sb) types was found. A brief discussion on the existence of a Holmberg Effect is also presented.

Key words. galaxies: spiral – galaxies: elliptical and lenticular, cD – galaxies: structure – galaxies: photometry – galaxies: interactions – galaxies: kinematics and dynamics

1. Introduction

Mixed morphology (E+S) pairs of galaxies from the Catalog of Isolated Pairs of Galaxies (KPG; Karachentsev 1972) have proven to be an appropriate local sample for the study of the influence of non-merger interactions on the properties of galaxies and their evolution (Hernández-Toledo et al. 2003). Among its advantages, its size, completeness, relatively unbiased selection and easy of interpretation as compared to (S+S) samples (Hernández-Toledo et al. 1999) can be mentioned. The old POSS morphological classification and a more recent and uniform re-classification from the Lyon-Meudon Extragalactic Database (LEDA) suggests that ∼20−25% of the KPG consist of a spiral/irregular paired with an elliptical/lenticular galaxy. This number is in excess of that expected under the assumption that mixed pairs form by random capture. Studies of the expected frequency of interacting systems based on their interpretation as the relics of gravitational interactions between galaxies indicate that, in regions of low density (typical of mixed pairs), the frequency goes down a few orders of magnitude compared to observations (Chatterjee 1987). There is a current debate about the origin of such pairs. If mixed pairs form in a common environment, and initial environmental conditions determine galaxy morphology, then a fraction of the order of 20−25% is a surprise. Either pair formation by random capture is more efficient than previously thought or an important fraction of (E+S) pairs are a by-product of the secular evolution of pairs and higher order structures.

Rampazzo & Sulentic (1992) proposed four scenarios to account for the large number of mixed pairs. The scenarios involve some apparent mixed pairs as: 1) "early-type" systems involving an E/S0 paired with an S0 misclassified as a spiral, 2) "disky" systems with a spiral and a S0, 3) systems with early type components showing tidally induced pseudo-spiral features, and 4) systems that might be the late stage in the coalescence of higher order systems (triplets or compact groups) with the elliptical component as the merged portion of an originally spiral rich system. In such cases the new E galaxies are expected to have a M/L similar to that of their parent galaxies (Wiren et al. 1996; Teerikorpi 2001). Notice that scenarios in 1) and 2) are based on morphological considerations while 3) and 4) are related to the origin of systems.

Scenario 3) would involve pseudo-spiral structures containing little or no evidence of substructures (gas/dust/emission

Send offprint requests to: A. Franco-Balderas,
e-mail: alfred@astroscu.unam.mx

⋆ Based on data obtained at the 0.84 m telescope of the Observatorio Astronómico Nacional (OAN), San Pedro Mártir, Baja California, México, operated by the Instituto de Astronomía, UNAM.

⋆⋆ Tables 1–3 and Figs. 3–12 are only available in electronic form at http://www.edpsciences.org

regions) typical of classical spirals. In this case, the corresponding color profiles are expected to show no important radial gradients.

Scenario 4) involves different possibilities:

a) Non-merging encounters, where the external isophotes show twisting and variations in ellipticity, coupled with the presence of disky or boxy isophotes ($a_4/a \neq 0$). In some circumstances, these systems may show evidence of shells or ripples.
b) Merging encounters, with two probable scenarios where boxy isophotes are expected as the result of two precursor galaxies of similar masses, and disky isophotes expected when the precursor galaxies have a large difference in masses (e.g. Naab & Burkert 2001). In this circumstances, these systems may also show evidence of shells or ripples.

With these scenarios in mind, Franco-Balderas et al. (2003; hereafter Paper I) presented multicolor broad band (*BVRI*) photometry for a first set of 11 mixed pairs drawn from the KPG catalog. From a similar analysis as the one presented in this paper, an important number of true mixed pairs (5/11) was found. The remaining pairs included 4 disky pairs (S0+S), 1 early-type pair (E+S0) and 1 spiral-irregular pair.

In the present paper, we continue analyzing the photometric and morphological properties of a second set of 10 mixed pair candidates from the original KPG catalogue with the aim to define the largest possible subset of true (E+S) pairs for more detailed studies of their structural parameters and the implications for their evolution in non-isolated environments.

We present B, V, R and I photometric data: total magnitudes, $(B-V)$, $(B-R)$, $(B-I)$ colors, surface brightness profiles, color profiles and geometric ($\epsilon = 1-b/a$, PA and a_4/a) profiles with emphasis on the morphology and its relation to the global photometric properties. We address the following questions:

1) Are most of the mixed pairs in the KPG catalogue really (E+S) pairs? The early POSS classification indicate that, from an original sample of 126 mixed pais, 38 are of (S0+S) type and 88 are considered as (E+S) pairs.
2) Is there evidence that the spiral structure in the disk components can arise from the interaction process? That structure could have at least three characteristics that might allow us to distinguish them from ordinary spiral structure: a) they would not be associated with an underlying disk component, b) they would be relatively featureless if they arose from a lenticular galaxy and c) the arms would be very open (integral sign) if produced fairly recently, since the winding effect of differential rotation would be small.
3) Is there any evidence of a correlation between the geometric profiles, the shape of color and surface brightness profiles, and the detailed morphology (bars, rings, shells, ripples, etc.) in these galaxies? Interactions are adequate to stimulate deviations from symmetry as evidenced by the presence of bars, rings, pseudo-rings and knotty structures along the arms and disks, while the presence of shells and ripples are presumably related to encounters and mergers in elliptical galaxies.

The structure of the paper is as follows. Section 2 summarize our photometric observations, reductions and uncertainty estimations. Section 3 presents the observational results in tabular, imaging and graphical form, including comments for individual objects. Section 4 is a general discussion of the results obtained on the light of current models and a test for the Holmberg effect, while Sect. 5 is a summary of our conclusions.

2. Observations and data reduction

The observations of the mixed pairs in this paper were carried out on April 2000 at Observatorio Astronómico Nacional (OAN) (San Pedro Mártir, Baja California). The CCD *BVRI* photometry (in the Johnson-Cousins system) was obtained with a SITE1 CCD detector attached to the 0.84 m telescope, covering an area of about $6.7' \times 6.7'$. The scale of the observations is $0.79''$/pixel.

Following Paper I, we have applied no special strategy in selecting this second subset of 10 mixed pairs. Available observing time and weather conditions were the main factors limiting the number of observed pairs. A journal of this second set of the photometric observations is given in Table 1. Column (1) gives the original catalogue number, Cols. (2)−(9) give the number of frames per filter, the integration time (in seconds) and seeing conditions (in $''$).

Images were debiased, trimmed, and flat-fielded using standard IRAF[1] procedures.

Photometric calibration was achieved by nightly observations of standard stars of known magnitudes from the Landolt lists (Landolt 1992). Standard stars with a color range $-0.29 \leq (B-V) \leq 0.69$ and $-0.30 \leq (V-I) \leq 0.84$ were observed. The main extinction coefficients and resulting parameters of the transformation (see Paper I), can be found in Table 2.

Table 3 gives some relevant information for the observed pairs from the literature. Column (1) is the KPG catalogue number, Cols. (2) and (3) reports other identifications and the apparent B magnitude from NED, Col. (4) is the projected separation of each pair in arc-minutes, and Col. (5) is the linear separation in kpc, Col. (6) the radial velocity for each component in km s^{-1} from NED, and finally, Col. (7) gives the major axis diameter, at $\mu_B = 25$, in kpc ($H_o = 75$ km s^{-1} Mpc^{-1}).

Total magnitudes were computed alternatively using polygonal apertures within POLYPHOT routines in IRAF. Foreground stars within the aperture were removed interactively. Elliptical surface brightness contours were fit using the STSDAS package ISOPHOTE in IRAF. We remind the reader that:

$$\frac{a_4}{a} = \frac{\sqrt{1-\epsilon}B_4}{a|\frac{dI}{da}|}$$

is a dimensionless measure of the isophotal shape, indicating whether a galaxy is boxy ($a_4/a < 0$) or disky ($a_4/a > 0$). For a detailed discussion see Milvang-Jensen & Jørgensen (1999).

[1] The IRAF package is written and supported by the IRAF programming group at the National Optical Astronomy Observatories (NOAO) in Tucson, Arizona. NOAO is operated by the Association of Universities for Research in Astronomy (AURA), Inc. under cooperative agreement with the National Science Foundation (NSF).

Table 4. Observed magnitudes.

KPG	*B*	*V*	*R*	*I*	Notes
KPG191A	15.40 ± 0.13	14.41 ± 0.08	13.76 ± 0.11	12.97 ± 0.12	
KPG191B	15.66 ± 0.13	14.62 ± 0.08	13.95 ± 0.11	13.02 ± 0.12	
KPG229A	14.46 ± 0.11	13.61 ± 0.06	13.07 ± 0.90	12.50 ± 0.10	
KPG229B	15.02 ± 0.11	14.24 ± 0.06	13.58 ± 0.09	12.68 ± 0.10	BS
KPG239A	14.50 ± 0.12	13.67 ± 0.07	13.08 ± 0.10	12.46 ± 0.10	
KPG239B	14.77 ± 0.12	13.99 ± 0.07	13.41 ± 0.10	12.66 ± 0.11	
KPG303A	12.82 ± 0.11	11.85 ± 0.07	11.24 ± 0.10	10.45 ± 0.10	
KPG303B	14.02 ± 0.11	13.14 ± 0.07	12.55 ± 0.10	12.17 ± 0.10	
KPG386A	15.44 ± 0.13	14.49 ± 0.08	13.94 ± 0.11	12.60 ± 0.12	
KPG386B	14.61 ± 0.13	13.65 ± 0.07	13.10 ± 0.11	12.30 ± 0.12	
KPG392A	14.12 ± 0.11	13.19 ± 0.07	12.58 ± 0.10	11.81 ± 0.10	BS
KPG392B	16.23 ± 0.11	15.70 ± 0.07	15.33 ± 0.10	14.63 ± 0.11	
KPG419A	12.84 ± 0.16	11.96 ± 0.09	11.43 ± 0.14	10.77 ± 0.15	
KPG419B	13.30 ± 0.16	12.46 ± 0.09	11.83 ± 0.14	11.08 ± 0.15	
KPG432A	14.50 ± 0.11	13.69 ± 0.07	13.11 ± 0.10	12.25 ± 0.10	
KPG432B	13.59 ± 0.11	12.95 ± 0.07	12.46 ± 0.10	11.81 ± 0.10	
KPG460A	14.32 ± 0.13	13.58 ± 0.08	13.00 ± 0.11	12.61 ± 0.12	
KPG460B	13.84 ± 0.13	12.98 ± 0.08	12.32 ± 0.11	11.67 ± 0.12	
KPG476A	14.93 ± 0.14	14.10 ± 0.08	13.47 ± 0.12	12.62 ± 0.12	
KPG476B	13.66 ± 0.14	13.01 ± 0.08	12.49 ± 0.12	11.77 ± 0.12	

BS = Bright Star Close/Superposed to a Galaxy.

Typical errors for the geometric parameters are $\Delta\epsilon = 0.05$, ΔPA = 7°, and $\Delta(a_4/a) \times 100 = 0.007$. Our derived parameters are generally in good agreement with those reported in RC3, aperture photometry catalogues and other individual photometric works, when available.

For more details concerning these procedures see Paper I.

2.1. Standard stars

An estimation of the errors in our photometry involves two parts: 1) the procedures to obtain instrumental magnitudes, and 2) the uncertainty when such instrumental magnitudes are transformed to the standard system. After a least square fitting, the associated errors to the slope in each principal extinction coefficient are shown in Table 2. An additional error δ(airmass) $\sim$ 0.005 from the airmass routines in IRAF was also considered. For 2), the zero point and first order color terms are the most important to consider.

A comparison of our CCD magnitudes against those reported in Landolt (1992) for 8 stars in common show no significant deviations. The internal errors can be described by a $\sigma_B \sim 0.034$, $\sigma_V \sim 0.033$, $\sigma_R \sim 0.033$ and $\sigma_I \sim 0.028$.

After transforming to the standard system by adopting our best-fit coefficients, the formal errors are also shown in Table 2. To estimate the total error in each band, it is necessary to use the transformation equations and then propagate the errors. The total typical uncertainties are 0.12, 0.08, 0.10 and 0.11 in *B*, *V*, *R* and *I* bands, respectively. However, see Table 4 for individual estimations.

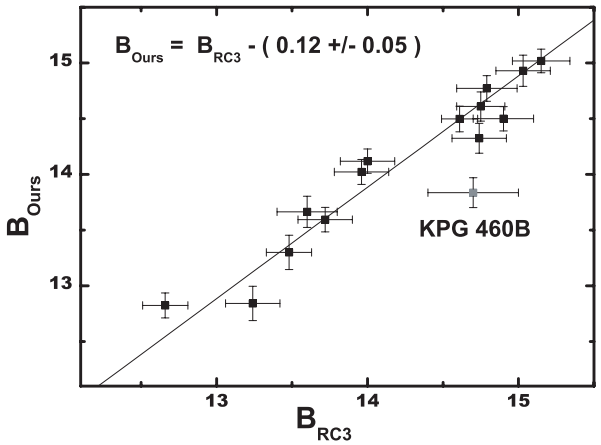

Fig. 1. Comparison between our total *B* and *V* magnitudes and total magnitudes from RC3 Catalogue.

2.2. Paired galaxies

A comparison of our total *B*-band magnitudes and those available in the RC3 Catalogue (de Vaucouleurs et al. 1991) is shown in Fig. 1.

Figure 1 shows that the agreement with reported total *B*-band magnitudes is good. The solid line in the plot shows

Table 5. Corrected magnitudes and color indices.

KPG	B_0	V_0	R_0	I_0	$(B-V)_0$	M_{B_0}	$(B-V)^0_T$	M^0_B
KPG191A	14.86 ± 0.13	14.03 ± 0.08	13.46 ± 0.11	12.75 ± 0.12	0.82 ± 0.15	−20.06	0.83 ± 0.15	−19.99
KPG191B	14.45 ± 0.55	13.63 ± 0.42	13.12 ± 0.30	12.40 ± 0.19	0.84 ± 0.69	−20.44	0.87 ± 0.15	−20.18
KPG229A	14.10 ± 0.11	13.39 ± 0.06	12.90 ± 0.09	11.92 ± 0.10	0.70 ± 0.12	−21.39	0.74 ± 0.12	−21.29
KPG229B	13.94 ± 0.56	13.34 ± 0.43	12.81 ± 0.30	12.08 ± 0.18	0.60 ± 0.70	−21.52	0.69 ± 0.12	−21.45
KPG239A	14.30 ± 0.12	13.57 ± 0.07	13.01 ± 0.10	12.40 ± 0.10	0.73 ± 0.13	−20.90	0.75 ± 0.13	−20.83
KPG239B	14.49 ± 0.16	13.77 ± 0.11	13.23 ± 0.12	12.50 ± 0.11	0.71 ± 0.20	−20.72	0.72 ± 0.13	−20.68
KPG303A	12.61 ± 0.11	11.71 ± 0.07	11.13 ± 0.10	10.37 ± 0.10	0.90 ± 0.13	−20.62	0.90 ± 0.13	−20.54
KPG303B	13.57 ± 0.24	12.77 ± 0.17	12.24 ± 0.15	11.96 ± 0.12	0.80 ± 0.29	−19.70	0.82 ± 0.13	−19.42
KPG386A	14.28 ± 0.73	13.46 ± 0.55	13.08 ± 0.39	11.87 ± 0.24	0.82 ± 0.91	−21.09	0.86 ± 0.15	−20.58
KPG386B	14.30 ± 0.13	13.47 ± 0.07	12.96 ± 0.11	12.20 ± 0.12	0.83 ± 0.15	−21.15	0.86 ± 0.15	−21.01
KPG392A	13.87 ± 0.11	13.04 ± 0.07	12.47 ± 0.10	11.73 ± 0.10	0.83 ± 0.13	−20.92	0.86 ± 0.13	−20.80
KPG392B	15.60 ± 0.49	15.18 ± 0.37	14.91 ± 0.27	14.31 ± 0.17	0.41 ± 0.62	−19.23	0.48 ± 0.13	−19.20
KPG419A	11.71 ± 0.82	10.92 ± 0.62	10.56 ± 0.44	10.13 ± 0.27	0.79 ± 1.03	−20.17	0.84 ± 0.18	−19.77
KPG419B	13.01 ± 0.16	12.24 ± 0.09	11.66 ± 0.14	10.96 ± 0.15	0.76 ± 0.18	−19.07	0.79 ± 0.18	−18.82
KPG432A	14.35 ± 0.11	13.60 ± 0.07	13.04 ± 0.10	12.19 ± 0.10	0.75 ± 0.13	−18.95	0.77 ± 0.13	−18.79
KPG432B	13.18 ± 0.28	12.59 ± 0.20	12.17 ± 0.16	11.59 ± 0.12	0.58 ± 0.34	−20.10	0.62 ± 0.13	−19.94
KPG460A	13.25 ± 0.60	12.67 ± 0.45	12.24 ± 0.32	12.05 ± 0.20	0.59 ± 0.75	−21.68	0.68 ± 0.15	−21.23
KPG460B	13.55 ± 0.13	12.82 ± 0.08	12.19 ± 0.11	11.58 ± 0.12	0.74 ± 0.15	−21.43	0.77 ± 0.15	−21.27
KPG476A	14.13 ± 0.62	13.37 ± 0.47	12.84 ± 0.34	12.14 ± 0.21	0.76 ± 0.77	−19.64	0.77 ± 0.16	−19.29
KPG476B	13.06 ± 0.34	12.50 ± 0.25	12.07 ± 0.20	11.45 ± 0.15	0.56 ± 0.42	−20.67	0.60 ± 0.16	−20.40

a fit by forcing a unity slope value. Then a typical displacement of −0.12 can be inferred from the data, consistent with our error estimations.

The only significant difference is for KPG460B. Our measure disagree by about 0.7 mag with respect to the value reported in RC3. The explanation for this is a bright foreground star superposed close to the galaxy center, avoiding an appropriated masking of its contaminating light. Notice, however, the large error bars reported in RC3.

Sources to compare our photometry of pairs in other bands than B are difficult to find. However, Prugniel & Heraudeau (1998) report total magnitudes for a few of our pair components: $V = 13.67$ for KPG239A, $V = 13.67$ for KPG303A, $V = 13.72$ for KPG432A and $B = 13.40$ for KPG432B. Da Costa et al. (1998) report $B = 13.55$ for KPG419B, Finally, Roth (1994) reports $I = 10.92$ for KPG419A, while Haynes et al. (1999) report $I = 12.04$ for KPG432B. All the above values are in agreement with our total uncorrected magnitudes, within the estimated errors.

3. Results

3.1. Integrated magnitudes and colors

The observed magnitudes and colors for individual galaxies in the sample are presented in Table 4. Entries are as follows: Col. (1) gives the identification in Karachentsev Catalogue, Cols. (2) to (5) give the total magnitudes in B, V, R and I bands, and Col. (6) gives some notes regarding to the presence of bright stars nearby in the field.

The individual corrected magnitudes and colors are presented in Table 5. Entries are as follows: Col. (1) gives the identification in Karachentsev Catalogue, Cols. (2) to (5) give the total corrected magnitudes in B, V, R and I bands, taking into account galactic blue absorptions from Schlegel et al. (1998), inclination corrections from Tully et al. (1998) with coefficients taken from Verheijen (2001) and K-corrections interpolated from Frei & Gunn (1994). Column (6) gives the corresponding corrected $(B-V)$ color. Column (7) gives the corresponding absolute blue magnitude, taking into account corrections in Col. (2). Column (8) gives the corrected $(B-V)^0_T$ color, according to RC3. Finally, Col. (9) gives the blue absolute magnitude applying corrections from RC3. Notice that the most important contribution to the total errors comes from applying a more physical correction due to inclination and self-absorption ΔA_i to late-type galaxies, in terms of absolute magnitudes, (cf. Verheijen 2001).

Our observations span a range (11.7−15.6) and (0.48−0.90) mag in B^0_T and $(B-V)^0_T$, respectively. The observed $(B-V)$ range is comparable to our first set of (E+S) pairs and other reported samples of interacting galaxies with similar observations (see Paper I and references therein).

3.2. Colors and morphology

To discuss the optical morphology and its relationship to the global photometric properties, the final results for each pair

are presented in the form of a mosaic (cf. Figs. 3–12). Each mosaic includes: 1) a *B*-band image, 2) a *B*-band filtered image, 3) *BVRI* surface brightness and color profiles, and 4) its corresponding geometric (radial ϵ, PA and a_4/a) profiles. In most of the cases, foreground stars in the field have been removed. We have carried out 1) a reclassification of the previous POSS/LEDA Hubble morphology, and 2) a classification of the spiral arm morphology as suggested by Elmegreen & Elmegreen (1982) (hereafter EE class), when possible.

As mentioned in Paper I, the evaluation of morphology took place in different steps: 1) evaluation of the geometrical profiles for the early-type components along with the surface brightness profiles, 2) evaluation of the geometric profiles that could give clues of arm-like, bar-like and ring-like features, with the help of filtered images, 3) evaluation of outer arms probably generated by tidal interactions.

We were interested on the early-type components to quantify the possible presence of disky structure. Although the absolute value of the geometrical parameter (a_4/a) depends on the inclination of the galaxy to the line of sight, its sign is useful for detecting subtle disky features in early-type components. The presence of disky isophotes is one criterion for assigning a galaxy to the lenticular class. However it is fair to remember that disky components are also found in E-types. With the purpose of distinguishing S0 candidates as well as ellipticals with boxy and disky structure, a galaxy in our sample was judged to be an elliptical if the surface brightness profile did not show any hint of an exponential outer component.

In addition, we identify a galaxy as barred if: 1) the ellipticity increases as a function of radius to a maximum and then decreases to reveal the inclination of the disk, and 2) the position angle is approximately constant over the radii where the ellipticity is rising. This depends on the prominence of the bar and on its relative orientation with respect to the global PA of the galaxy disk.

The combination of *B* band, *B*-filtered images, surface brightness and color profiles as well as geometric profiles are a powerful technique for morphological classification and for revealing fine structural details most likely related to encounters that are in various early and late stages.

The discussion of morphological types also uses the information on the estimated mean colors $(B-V)_0^T$. Median integrated total $(B-V)$ colors of galaxies according to morphological class are given by Roberts & Haynes (1994). The UGC and the Local Supercluster (LSc) samples in Roberts & Haynes (1994) are rather inhomogeneous in terms of environment, but the interacting objects were excluded from their analysis and we may consider these samples as comparison/reference samples for the following discussion.

3.3. Comments on individual objects

From Table 3, notice that the mixed pairs in this study show a projected mean separation $\Delta x \sim 67$ kpc. This value is ∼67% higher than the mean for the entire KPG mixed pair sample ($\Delta x \sim 40$ kpc). Similarly, notice that five out of ten pairs have radial velocities in excess of the representative mean ($V_{\rm rad} \sim 6500\,{\rm km\,s^{-1}}$) of the mixed sample. These facts, coupled with the small angular size of the galaxies, are limiting our ability to resolve and describe morphological details.

KPG191. This is an isolated system showing no obvious signs of interaction beyond possible distortions internal to the galaxies. **Component A:** evidence for a disk structure is seen in the a_4/a and μ profiles. The PA and ϵ profiles show evidence of a precessing structure (bar?/arms?) along the disk. We classify this galaxy as a SAB0 pec. The total $(B-V)_T^0$ color is more representative of E/S0 types. **Component B:** a prominent bulge and two nearly symmetric and structureless arms are observed in the μ and color profiles. Arms can be traced by the PA and ϵ profiles and may be interpreted as the result of the interaction. We classify this galaxy as a Sa pec. The total $(B-V)_T^0$ color is more representative of E/S0 types. The *B*-filtered image shows the presence of dust lanes that may be contributing to the reddening in colors. Our EE class is 8.

KPG229. This is the pair with the major apparent separation and larger recessional velocity. **A:** the μ and a_4/a profiles show evidence of an external disk and/or a diffuse envelope after the first 10″. We classify this galaxy as an E(3−4)/S0. The total $(B-V)_T^0$ color is more representative of S0/Sa types. **B:** two tight arms in the inner regions and more asymmetric open arms (probably of tidal origin) in the external regions are follow closely by the geometric profiles. We classify this galaxy as a Sb pec. The total $(B-V)_T^0$ color is more representative of Sab/Sb types. Our EE class is 5.

KPG239. This is not an isolated system. The *B*-band image shows several galaxies in the field from which the galaxies in KPG239 are the most prominent. **A:** the geometric profiles show evidence of disky structure in the inner 17″ suggested by the a_4/a profiles. After 17″, a diffuse envelope is also detected. We classify this galaxy as a E3/S0 pec. The total $(B-V)_T^0$ color is more representative of S0/Sa types. **B:** the *B*-band filtered image clearly shows a set of tightly wrapped and prominent arms forming a ring and a lopsided external arm at the south that can be traced in the geometric profiles. Previous classifications suggest the presence of a bar not visible in our images. We classify this galaxy as a Sb pec. The total $(B-V)_T^0$ color is consistent with Sa/Sab types. Our EE class is 6, however see Elmegreen & Elmegreen (1982).

KPG303. This system is forming an apparent triplet with MCG +10-17-075 (major axis at 25 mag/arcsec^2 ≃ 30″, and $B_{\rm tot}$ = 17.1 mag). **A:** our geometric profiles are consistent with those reported in Bender et al. (1988) within the inner 30″. They classify this galaxy as a E, however, after 30″ we observe evidence for a disk structure in our a_4/a and μ profiles (notice that to have a comparable a_4/a quantity, it is necessary to eliminate the normalization factor $(a|\frac{{\rm d}I}{{\rm d}a}|)$ in our definition). Nieto et al. (1994) classify this galaxy as an "elongated E4". We classify this galaxy as E4/S0 pec. The total $(B-V)_T^0$ color is consistent with E/S0 types. **B:** the geometric profiles show three definite regions that can be associated with the following structures: 1) a prominent elongated bulge; 2) a strong superposed bar, from which; 3) tightly wound structureless spiral arms apparently emerge. The arms may be interpreted as the result of the interaction process. We classify this

galaxy as a SB(rs)a. The total $(B-V)_T^0$ color is consistent with S0/Sa types. Our EE class is 10.

KPG386. **A:** this is an inclined spiral galaxy showing the presence of strong dust lanes (visible in the *B*-band filtered image), that may be contributing to the reddening in colors. A moderated bulge and two adjacent symmetric arms (that subsequently broaden out in the external region), can be traced with our geometric profiles. We classify this galaxy as a Sab pec. The total $(B-V)_T^0$ color is consistent with S0/Sa types. Our EE class is 5. **B:** an elongated bulge and evidence of a subjacent disk (with faint precessing structure) are observed in the μ and geometric profiles. We classify this galaxy as a E3/SAB0 pec. The total $(B-V)_T^0$ color is consistent with E/S0 types.

KPG392. **A:** an elongated central bar-like structure is observed in our geometric profiles while the μ profile shows evidence of a disk in the external region (with a faint two-fold spiral-like structure). We classify this galaxy as a SAB0/SABa. The total $(B-V)_T^0$ color is consistent with S0/S0a types. **B:** the bulge is visible in the *B*-band image. The μ and a_4/a profiles support the disky nature of the isophotes and may be suggesting the presence of subjacent structure. At the resolution of our observations, the angular size of this galaxy and its inclination do not allow a more detailed morphological classification. The corresponding morphological type is Scd/Sd (based only on its mean corrected color). The color profiles show evidence of a starburst episode.

KPG419. **A:** this is a highly inclined galaxy with a complex morphology. The geometric profiles are clearly dominated by a linear structure (a peanut-like bar) all along the disk. This structure resembles the results of simulations about gas-driven evolution of stellar orbits in barred galaxies (Berentzen et al. 1998). Our images suggest a complex interplay between the tightness of the arms an a set of dust lanes that may be contributing to the reddening in colors. The μ profiles, in combination with our images suggest that the bulge component is compact. We classify this galaxy as a SBb pec. The total $(B-V)_T^0$ color is consistent with S0/S0a types. Notice the faint object (a galaxy?) to the north-east. **B:** a conspicuous bulge region is observed in the geometric profiles while the μ profiles show the presence of a disk. We classify this galaxy as a S0 pec. The total $(B-V)_T^0$ color is consistent with S0a/Sa types.

KPG432. **A:** Rest et al. 2001 describe the HST nuclear light distribution (inner 10″) with a power law. The geometric profiles are consistent with a face-on compact nuclei galaxy and an external disk, visible in μ profiles (resembling a Zwicky compact object). Subjacent structure (not visible in our images) may be inferred from our geometric profiles. We observe a faint object (a galaxy?) at west. We classify this galaxy as a S0. The total $(B-V)_T^0$ color is consistent with S0a/Sa types. **B:** the multi-arm spiral pattern dominates the behavior of the geometric profiles. Two prominent arms delineated by star formation regions seem to emerge from an inner ring-like structure. At our resolution, the inner region resembles either an elongated bulge or a barred structure. We classify this galaxy as a S(rs)c. The total $(B-V)_T^0$ color is consistent with Sb/Sbc types. Our EE class is 6.

KPG460. This pair is revealed forming an apparent triplet with MCG +13-11-12 (major axis $\simeq$ 36″ at the isophote 25 mag/arcsec^2, and $B_{\rm tot}$ = 15.1 mag). **A:** this is a highly inclined spiral galaxy with the presence of a dust lane (from the north-east to the south-west edge) that makes it difficult to trace the shape of the arms. Both the north-eastern and south-western edges show evidence of features most probably of tidal origin, giving the appearance of a warped disk. We classify this galaxy as a Sb pec. The total $(B-V)_T^0$ color is consistent with Sab/Sb types. **B:** after masking the field star near the center, two possible sources of light contamination still remain: 1) the remnant light from the masked star, and 2) the light contamination from the nearby companion (notice the high dispersion shown by the a_4/a profile in the external region). After taking this into account, we tentatively classify this galaxy as E2. The total $(B-V)_T^0$ color is consistent with S0a/Sa types.

KPG476. **A:** the high inclination of this galaxy makes it difficult to trace detailed morphological features. A small bulge component and an extended disk are visible in our μ and geometric profiles. A filamentary structure at the edge of the galaxy is detected in the a_4/a profiles. The total $(B-V)_T^0$ color is consistent with Sa/Sab types. Notice that our *B*-band filtered image may be suggesting an edge-on spiral. We classify tentatively this galaxy as a Sab pec. **B:** this is an ocular galaxy with two prominent spiral arms (delineated by star formation regions), going to the central region and simulating an elongated ring that encloses a blue prominent bulge and a subjacent bar-like structure. We classify this galaxy as a SB(rs)b pec. The total $(B-V)_T^0$ color is consistent with Sb/Sbc types. Our EE classification is 10. Notice the peculiar linear structure that seems to cross the bulge region at a PA $\simeq -45°$ (see *B*-band filtered image).

4. Discussion

This paper represents a second part of a more detailed analysis of the properties of mixed pairs in forthcoming papers. In this section we follow closely Rampazzo & Sulentic (1992).

Comparing the results in Paper I where we found 5 true (E+S) pairs, in this study we find 1 true (E+S) pair and 4 probable (E+S) pairs ((E/S0+S) cases). Additionally, we find 3 lenticular-spiral (S0+S) systems (scenario 2 in Rampazzo & Sulentic 1992), 1 spiral-spiral (S+S) system and 1 probable spiral-spiral system ((S0/Sa+S) case).

Early type components show evidence of underlying (perhaps induced) structure like bars (KPG386B and KPG392A), twisting (KPG191A, KPG239A, KPG386B and KPG392A), or both. Additionally KPG386B and KPG392A show hints of probably induced arms (falling in scenario 3).

In most cases the morphology of the late type component is less ambiguous. However, cases like KPG386A, KPG419A and KPG460A show confusion because the structures on the disks are not clearly seen due to inclination effects and the presence of strong dust lanes. In the case of KPG392B the morphological classification is based only upon the mean colors. We do not have Irregulars in the present sample, confirming the rarity of these types of galaxies in our sample.

Candidates for tidally-generated spiral structure in the late-type components are KPG191B and KPG303B. Other cases

Table 6. Final results from this study.

Name	Hubble type (NED)	Hubble type (this work)	EE class	Isolation	Profile	Notes
KPG191A	S0	SAB0 pec			F	B, TA?
KPG191B	Sb	Sa pec	8			TA
KPG229A	E	E(3-4)/S0				
KPG229B	S?	Sb pec	5			TA
KPG239A	E?	E3/S0 pec		ADCG		
KPG239B	SABbc: (X-ray source)	Sb pec	6	ADCG		K, TA
KPG303A	E4-5 WLGR (Blazar)	E4/S0 pec		ACGC	F	
KPG303B	SB(rs)a	SB(rs)a	10	ACGC		B, R
KPG386A	Sa-b	Sab pec	5			TA
KPG386B	S0-	E3/SAB0 pec			F	B
KPG392A	S0	SAB0/SABa			F	B, TA?
KPG392B	Sb	Scd/Sd				
KPG419A	Sa pec sp (Sy 1.9)	SBb pec		ADCG		B
KPG419B	SAB(r)0	S0 pec		ADCG		
KPG432A	S?	S0			F	
KPG432B	SAB(rs)c	S(rs)c	6			R, K, TA
KPG460A	Sb	Sb pec		ACGC		TA?
KPG460B	E?	E2		ACGC	F	
KPG476A	S0? sp	Sab pec				
KPG476B	SBbc?	SB(rs)b pec	10		+	B, K, R

ADCG = Apparent Dwarf Companion Galaxy in the Filed.
ACGC = Apparent Companion Galaxy of Comparable Size.
B = Bar. K = Knot. R = Ring. TA = Tidal Arms.
F = Flat Color Profile. + = Positive Gradient in Color Profile.

like KPG229B and KPG239B show evidence of faint outer spiral structure apparently as a continuation of a more definite inner spiral structure.

The degree of isolation is another important point to consider for the origin and morphology in mixed pairs. Notice that in Table 6, 4 out of 10 pairs are not apparently isolated systems, however they were included in the Karachentsev catalogue since the apparent magnitude of the neighbor galaxies are fainter than the limit magnitude in that catalogue (15.7 mag). We do not have radial velocities to confirm their association.

Following Elmegreen & Elmegreen (1982), we succeeded in classifying 7 spirals. Some of the spirals in this sample are nearly edge-on, strongly interacting or simply do not fit into the Elmegreen & Elmegreen classes.

Interestingly, 6 galaxies out of 20 (30%) show evidence of barred structure and none are associated to spiral galaxies later than Sb (4 of them show a flat or positive gradient in color profiles). An over-representation of early Sa-Sb types is present. Only 2 galaxies classified as late-type (Sbc or later) were found. At this point, we caution the reader that part of this over-representation may well be due to our lacking of resolution. However, an alternatively possibility is that this may be evidence of a "nurture" scenario in pairs (Martinet 1995).

Similarly, about 16% of the disky components show evidence of ringed structure. These results could be interpreted in the framework of the simulations of Noguchi (1990 and references therein).

The filtered images presented here have been shown to be a powerful tool to disentangle galaxy morphology. The procedure behind is called Background Filtering (BGF). (cf. Sofue 1993). With this method, it is possible to study morphological structures in greater detail, which are detected in the original data but are embedded in bright foreground and background emission. The method is particularly useful to investigate morphological structures in the central regions of galaxies and also fainter details in the outskirts (see Paper I).

4.1. The Holmberg effect

Holmberg (1958) compared the photographic colors of paired galaxies and found a significant correlation between the colors of pair components. This phenomenon has since been referred to as the "Holmberg effect".

A physical explanation for the Holmberg effect is complex and it has been interpreted as: 1) evidence that similar types of galaxies form together (morphological concordance), because local environment determines galaxy morphology. It might also

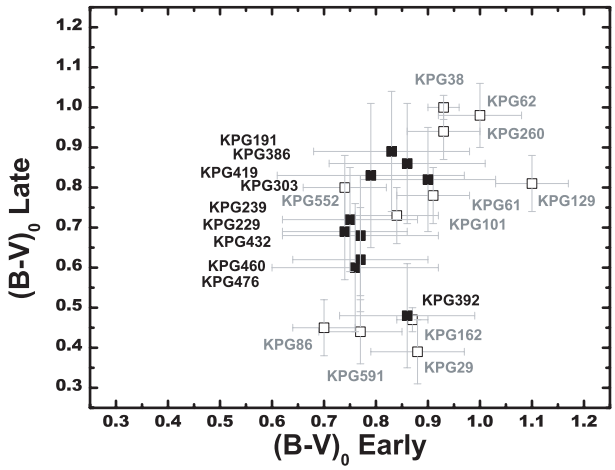

Fig. 2. The Holmberg effect. $(B-V)^0_T$ early-type galaxy versus $(B-V)^0_T$ late-type galaxy. Data from this work (filled squares). Data from Paper I (open squares).

reflect, 2) synchronized star formation histories in the pair components (Kennicutt et al. 1987). Notice that a Holmberg effect has also been reported in (E/S0+S) pairs (cf. Demin 1984).

In order to look for such an effect, after re-evaluating the morphological classification, we compare in Fig. 2 the $(B-V)^0_T$ color indices of components in the present sample. The color index along the vertical axis refers to the late type component and that along the horizontal axis refers to the early type component in each pair. In order to reinforce any possible correlation, besides showing the data in the present sample, the data from Paper I are also included. For the present sample,note that three of our pairs are concordant in type ($\Delta T \leq 2$), while the rest are morphological discordant ($\Delta T > 3$). Although we see some evidence for a trend between colors of the early and late type components, we caution the reader for the small number of data.

For the purpose of the discussion, Fig. 2 is broadly separated into two color regions:

1) Redder region above $(B-V)_0$Late ≥ 0.75 might be predicted to involve pairs without spiral components later than approximately Sab. We find it to be mainly composed of pairs with components of similar morphological type and colors (KPG191, KPG303, KPG386 and KPG419) meaning that some of them may not be true (E+S) binaries. Notice that when the data from Paper I is included, a wider scatter in color appears. Our Holmberg diagram is useful to test and reevaluate our classifications based on our geometric parameters and surface brightness profiles. For example, KPG303B shows a disk/bulge ratio near 0.5. It shows evidence for tightly wrapped arms but, there is no evidence of the fine structures due to dust and HII regions expected in spiral galaxies. These facts, in addition to its locus in our diagram, suggest that KPG303B may be consistent with a more early type classification (S0) with interaction induced structures.
2) A blue region ($(B-V)_0$Late ≤ 0.75), on the other hand, might be predicted to involve pairs without spiral components early than approximately Sab leading us to predict that true (E+S) pairs will be found here (KPG229, KPG239, KPG432, KPG460 and KPG476). Most of the pairs that we classify as (E+S) are indeed found here. The location of KPG476A in the blue region placed the original S0 classification into question. Its color suggest a more late type classification which might be more consistent with a disk/bulge ratio near 0.2. Thus, we considered KPG476 as a (S+S) pair.

KPG392 appears to be an outlier in Fig. 2 but it shows a color combination with a true mixed pair (the same case for KPG29 and KPG162 from Paper I). Naturally we expect the blue region of pairs to show a larger dispersion, especially in the vertical direction, reflecting the wider dispersion in colors across the spiral components. KPG392B is about 4.74 times fainter than its primary, with a very blue color consistent with a Sc-d types. A similar case of a hierarchical pair is KPG591 (see Paper I).

KPG476 and KPG591 (the only spiral-spiral or spiral-irregular pairs in our samples) were also included in Fig. 2 to illustrate their position in the Holmberg diagram.

Some of the true (E+S) pairs show color correlation. A possible explanation of this effect is mass transference from the S to the E component (Domingue et al. 2003).

The evidence of a Holmberg effect is marginally present, however, a more definite correlation can be expected after incorporating our additional observations in forthcoming papers.

5. Summary

Table 6 is a summary of the morphological features found in this work. Column (1) gives the pair catalogue number, Col. (2) gives the Hubble Type as reported in NED, Col. (3) gives the Hubble Type as estimated in this work, Col. (4) gives the Elmegreen (EE) class, Col. (5) indicates when other galaxies (dwarfs or galaxies of comparable size) are in the neighborhood of the pair, Col. (6) indicates when a flat or positive gradient color profile is present, and finally Col. (7) indicates the presence of rings, bars and knotty structures.

There are two confirmed AGN (a Blazar and a Seyfert 1.9) and one probable AGN (KPG239A; a strong X-ray source in Henriksen & Cousineau 1999) in this sample. It is generally believed that a high percentage of Seyfert galaxies have close neighbors implying an AGN-interaction connection (cf. Dultzin-Hacyan et al. 1999). The presence of these galaxies in mixed pairs (3/22) from Paper I and 3/20 in the present paper, supports the notion that the triggering mechanism for their nuclear activity is of tidal origin and that it does not depend strongly on the type of perturbing galaxy. A larger and more complete sample has been observed and will be used in forthcoming papers to address the relevant questions in a more significant way. The present sample of 10 pairs is not statistically significant and it is biased for some of the wider and farther pairs within the sample. The pairs not classified as true or probable (E+S) pairs are disky pairs composed of spiral and lenticular components. The high fraction of (Sa−Sb) components rises interesting questions about galaxy evolution suggesting that a "nurture" scenario may be playing an important role in mixed pairs.

Acknowledgements. A.F.B. and H.H.T. thank the staff of the Observatorio Astrónomico Nacional for assistance during the observations. A.F.B. acknowledges CONACyT for a scholarship. D.D-H. acknowledges support through grant IN115599 from DGAPA, PAPIT, UNAM. A.F.B. and H.H.T. thank I. Shlosman and L. Sparke for fruitful discussions. We specially thank the referee J.W. Sulentic for his valuable comments and major contribution to the improvement of this paper. We have made use of NED and LEDA databases throughout this paper.

References

Bender, R., Döbereiner, S., & Möllenhoff, C. 1988, A&AS, 74, 385
Berentzen, I., Heller, C. H., Shlosman, I., & Fricke, K. J. 1998, MNRAS, 300, 49
Chatterjee, T. K. 1987, Ap&SS, 135, 131
Da Costa, L. N., Willmer, C. N. A., Pellegrini, P. S., et al. 1998, AJ, 116, 1
Demin, V. V., Zasov, A. V., Dibai, E. A., & Tomov, A. N. 1984, SvA, 28, 367
de Vaucouleurs, G., de Vaucouleurs, A., Corwin, H. G., et al. 1991, Third Reference Catalogue of Bright Galaxies (New York: Springer-Verlag)
Domingue, D. L., Sulentic, J. W., Xu, C., et al. 2003, AJ, 125, 555
Dultzin-Hacyan, D., Krongold, Y., Fuentes-Guridi, I., & Marzianni, P. 1999, ApJ, 513, L111
Elmegreen, B. G., & Elmegreen, D. M. 1982, MNRAS, 201, 1021
Franco-Balderas, A., Hernández-Toledo, H. M., Dultzin-Hacyan, D., & García-Ruiz, G. 2003, A&A, 406, 415
Frei, Z., & Gunn, J. E. 1994, AJ, 108, 1476
Haynes, M. P., Giovanelli, R., Salzer, J. J., et al. 1999, AJ, 117, 1668
Henriksen, M., & Cousineau, S. 1999, ApJ, 511, 595
Hernández-Toledo, H. M., Dultzin-Hacyan, D., González, J. J., & Sulentic, J. W. 1999, AJ, 118, 108
Herández-Toledo, H. M., Avila-Reese, V., Dultzin-Hacyan, D., & Sulentic, J. W. 2003, A&A, in preparation
Holmberg, E. 1958, Lund Medd. Astron. Obs. Ser. II, 136, 1
Karachentsev, I. D. 1972, Catalogue of Isolated Pairs of Galaxies in the Northern Hemisphere, Comm. Spec. Ap. Obs., 7, 1
Kennicutt, R. C., Roettiger, K. A., Keel, W. C., van der Hulst, J. M., & Hummel, E. 1987, AJ, 93, 1011
Landolt, A. U. 1992, AJ, 104, 340
Martinet, L. 1995, in Fundamentals of Cosmic Physics (Overseas Publishers Association), 15, 341
Milvang-Jensen, Bo., & Jørgensen, I. 1999, Baltic Astron., 8, 535
Naab, T., & Bukert, A. 2001 [astro-ph/0110179]
Nieto, J.-L., Poulain, P., & Davoust, E. 1994, A&A, 283, 1
Noguchi, M. 1990, in Paired and Interacting Galaxies, IAU Colloq., 124, 711
Prugniel, P., & Heraudeau, P. 1998, A&AS, 128, 299
Rampazzo, R., & Sulentic, J. W. 1992, A&A, 259, 43
Rest, A., Van den Bosch, F., Jaffe, W., et al. 2001, AJ, 121, 2431
Roberts, M. S., & Haynes, M. P. 1994, ARA&A, 32, 115
Roth, J. 1994, AJ, 108, 862
Schlegel, D. J., Finkbeiner, D. P., Douglas, P., & Davis, M. 1998, ApJ, 500, 525
Sofue, Y. 1993, PASP, 105, 308
Teerikorpi, P. 2001, A&A, 371, 470
Tully, R. B., Pierce, M. J., Huang, J.-S., et al. 1998, AJ, 115, 2264
Verheijen, M. A. W. 2001, ApJ, 563, 694
Wiren, S., Zheng, J.-Q., Valtonen, M. J., & Chermin, A. 1996, AJ, 111, 160

Online Material

Table 1. Journal of observations.

Galaxy pair	T_B (s)	$\langle B\rangle_{\rm FWHM}$ ($''$)	T_V (s)	$\langle V\rangle_{\rm FWHM}$ ($''$)	T_R (s)	$\langle R\rangle_{\rm FWHM}$ ($''$)	T_I (s)	$\langle I\rangle_{\rm FWHM}$ ($''$)
KPG191	2×1200	2.3	3×360	2.7	3×180	2.7	3×120	2.1
KPG229	2×1800	1.9	3×600	1.8	3×200	1.9	3×120	1.7
KPG239	2×1500	2.1	3×480	2.2	3×240	2.2	3×120	2.0
KPG303	2×600	2.1	3×240	2.2	3×120	2.1	3×60	1.9
KPG386	2×960	1.7	3×240	2.0	3×120	2.0	3×120	2.1
KPG392	2×3000	1.9	3×600	1.9	3×300	1.7	3×180	1.7
KPG419	2×2700	1.8	2×300	2.0	2×300	2.2	2×120	2.2
KPG432	2×1800	2.1	2×600	2.2	3×360	2.1	3×240	1.9
KPG460	2×2100	1.7	3×480	1.7	3×210	1.7	3×150	1.7
KPG476	2×1200	1.7	2×600	1.8	3×180	1.7	2×120	1.7

Table 2. Extinction and calibration coefficients for the optical observations.

April 2000			
Extinction coefficients			
k_b	k_v	k_r	k_i
0.273 ± 0.052	0.176 ± 0.045	0.121 ± 0.042	0.083 ± 0.044
Calibration Coefficients			
α_o	α_1	β_o	β_1
$2.456\ \pm0.040$	0.014 ± 0.067	0.487 ± 0.003	0.895 ± 0.006
ϵ_o	ϵ_1	γ_o	γ_1
$0.170\ \pm0.004$	1.068 ± 0.012	-0.092 ± 0.016	1.063 ± 0.023

Table 3. General (NED) data for the observed galaxies.

KPG number	Identif.	B mag	x_{1-2} ($'$)	x_{1-2} (kpc)	$V_{\rm rad}$ (km s^{-1})	A_{25} (kpc)
KPG191A	PGC 025935	15.60	0.64	17.9	7086 ± 70	16.6
KPG191B	PGC 025934	15.60			7059 ± 70	19.0
KPG229A	PGC 030011	15.10	4.57	165.3	9238 ± 30	43.4
KPG229B	UGC 05548	15.15			9387 ± 44	42.7
KPG239A	NGC 3286	14.61	3.92	125.2	8094 ± 47	52.4
KPG239B	NGC 3288	14.79			8151 ± 56	33.9
KPG303A	NGC 3894	12.66	2.03	26.4	3223 ± 19	28.3
KPG303B	NGC 3895	13.96			3159 ± 27	19.5
KPG386A	UGC 08595	15.70	1.97	69.5	8941 ± 57	30.0
KPG386B	NGC 5262	14.75			9181 ± 21	45.2
KPG392A	UGC 08689	14.00	5.03	134.1	6886 ± 60	42.9
KPG392B	PGC 048701	15.70			6955 ± 30	18.4
KPG419A	NGC 5506	13.24	3.82	27.7	1853 ± 8	13.6
KPG419B	NGC 5507	13.48			1852 ± 21	11.9
KPG432A	IZw 093	14.90	3.35	44.4	3256 ± 23	12.8
KPG432B	UGC 09476	13.72			3262 ± 8	17.7
KPG460A	NGC 5909	14.74	0.79	22.6	7052 ± 79	29.3
KPG460B	NGC 5912	14.70			7233 ± 23	35.7
KPG476A	NGC 6068A	15.03	1.98	32.4	3996 ± 58	15.3
KPG476B	UGC 10126	13.60			3975 ± 11	23.4

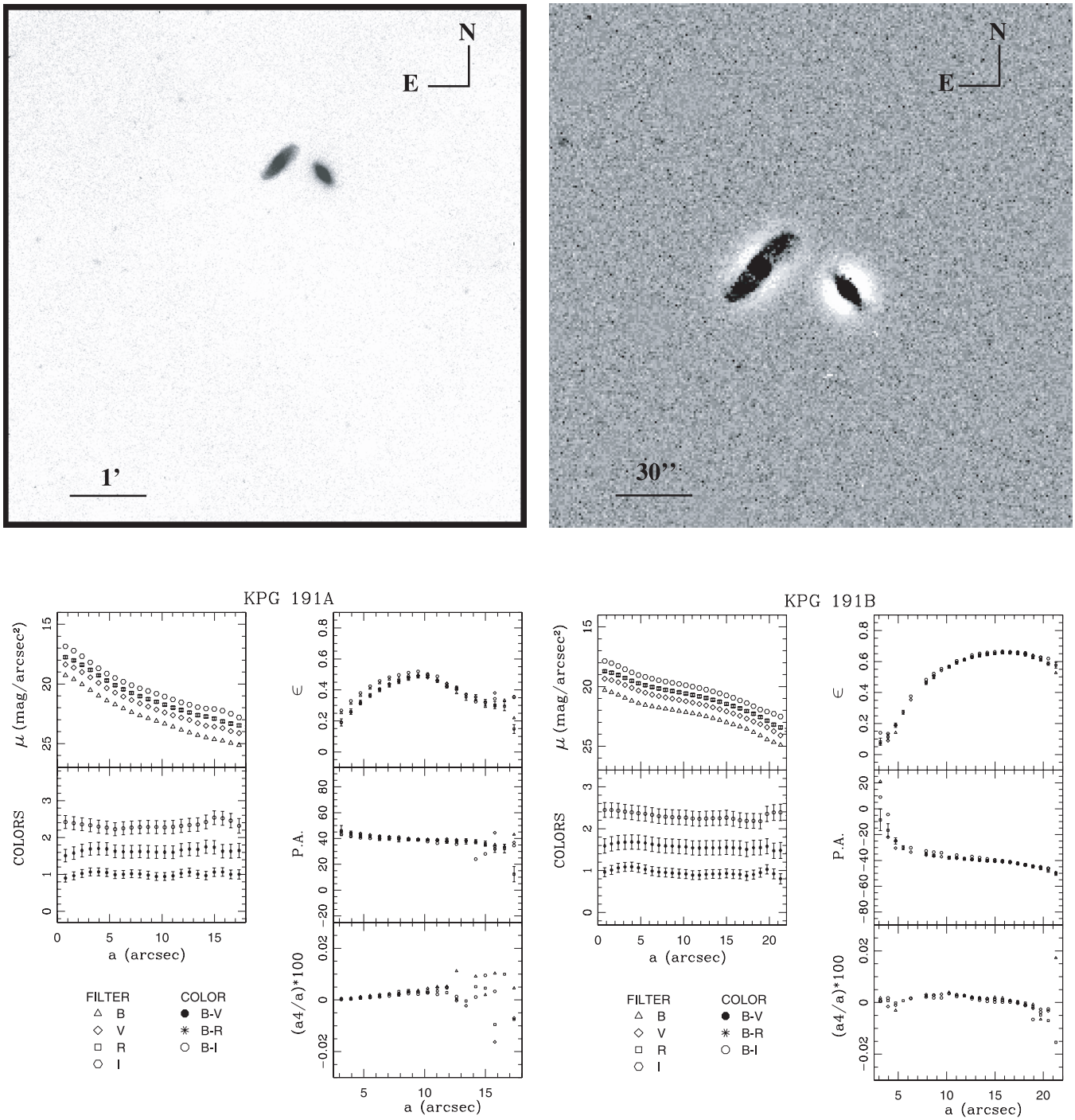

Fig. 3. KPG191 Mosaic. *Top left*: *B*-band image. *Top right*: *B*-band filtered image. *Bottom left*: surface brightness profile and geometric parameters for KPG191A. *Bottom right*: surface brightness profile and geometric parameters for KPG191B.

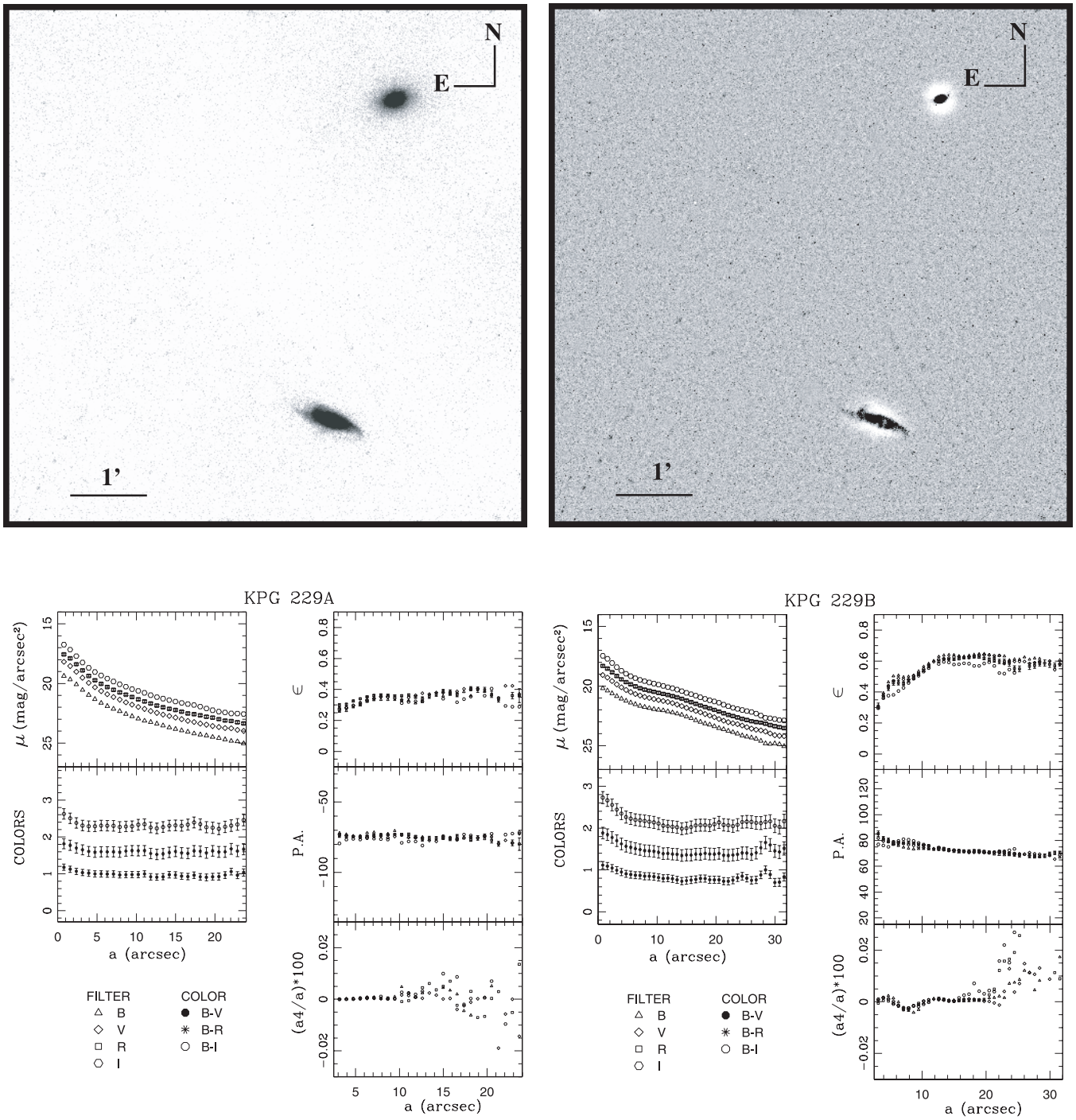

Fig. 4. KPG229 Mosaic. *Top left*: *B*-band image. *Top right*: *B*-band filtered image. *Bottom left*: surface brightness profile and geometric parameters for KPG229A. *Bottom right*: surface brightness profile and geometric parameters for KPG229B.

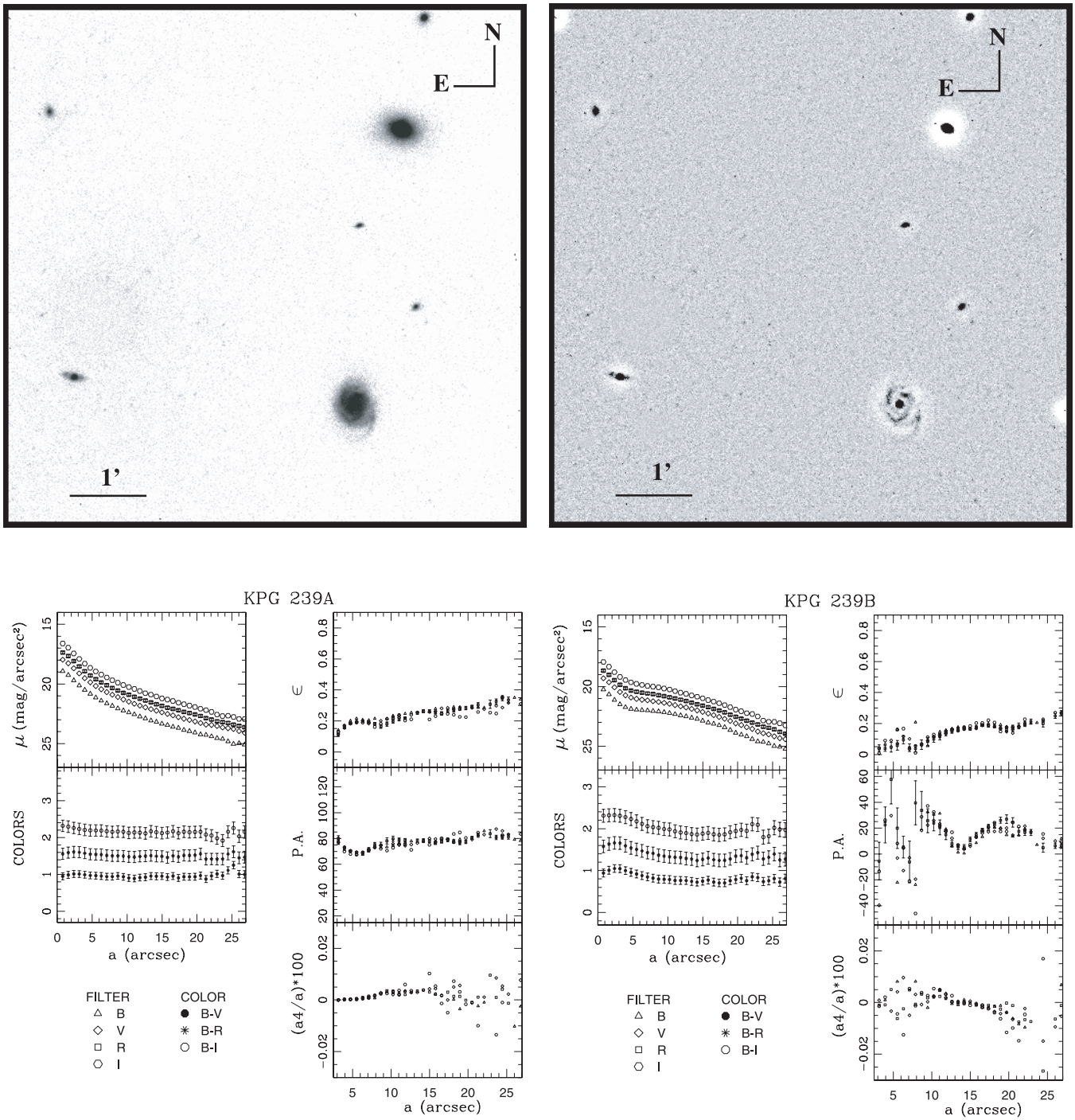

Fig. 5. KPG239 Mosaic. *Top left*: *B*-band image. *Top right*: *B*-band filtered image. *Bottom left*: surface brightness profile and geometric parameters for KPG239A. *Bottom right*: surface brightness profile and geometric parameters for KPG239B.

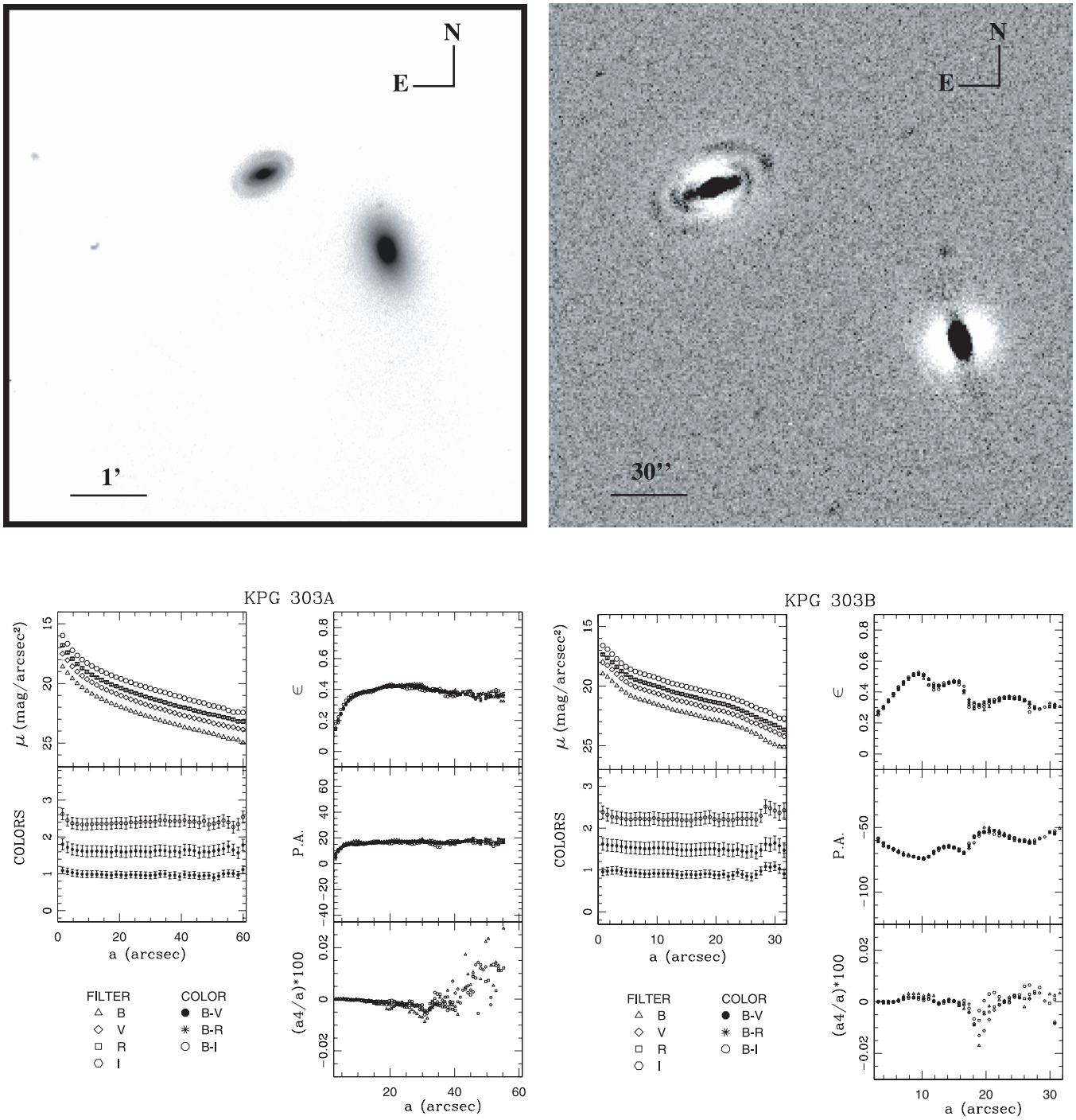

Fig. 6. KPG303 Mosaic. *Top left*: *B*-band image. *Top right*: *B*-band filtered image. *Bottom left*: surface brightness profile and geometric parameters for KPG303A. *Bottom right*: surface brightness profile and geometric parameters for KPG303B.

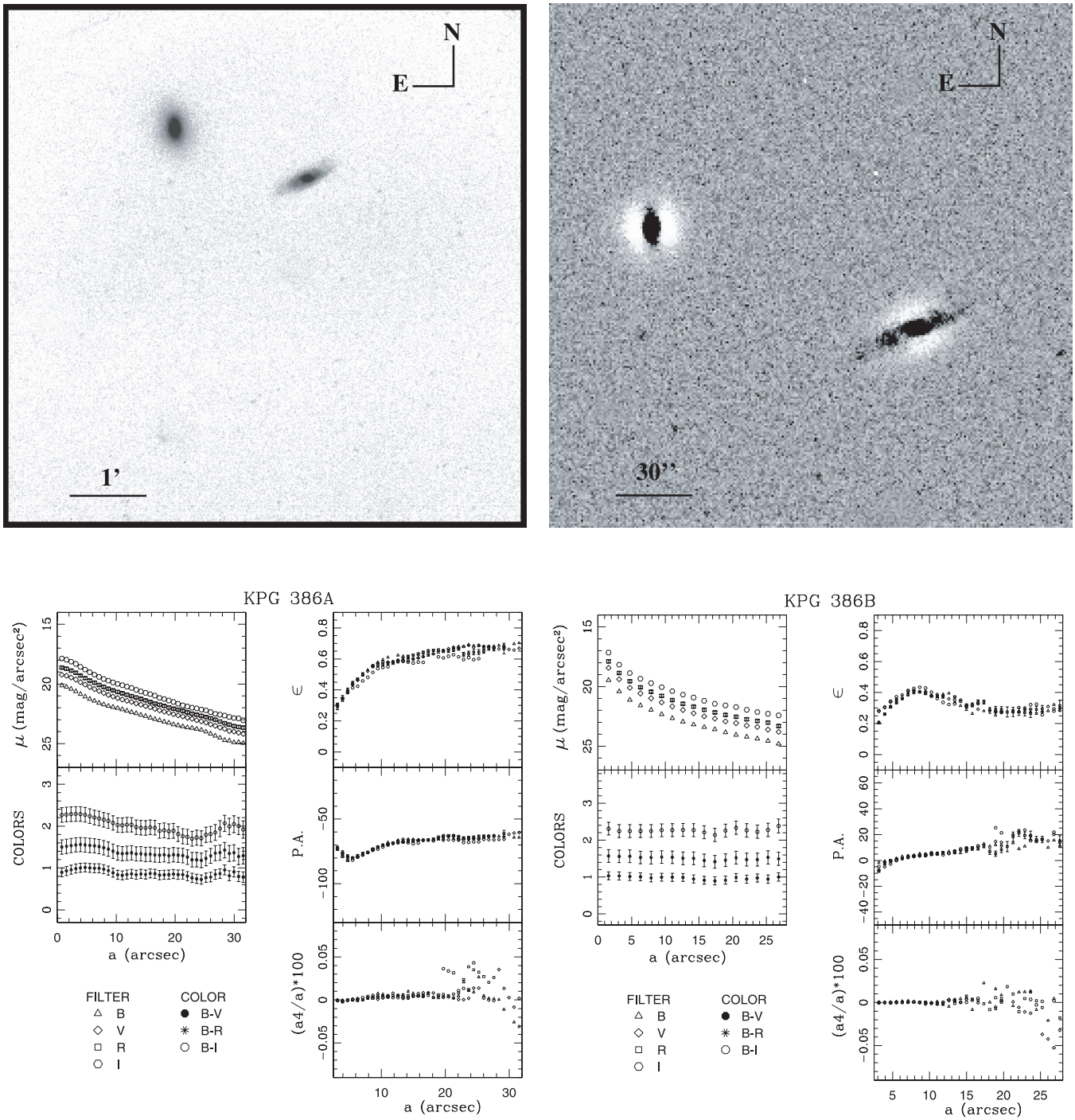

Fig. 7. KPG386 Mosaic. *Top left*: *B*-band image. *Top right*: *B*-band filtered image. *Bottom left*: surface brightness profile and geometric parameters for KPG386A. *Bottom right*: surface brightness profile and geometric parameters for KPG386B.

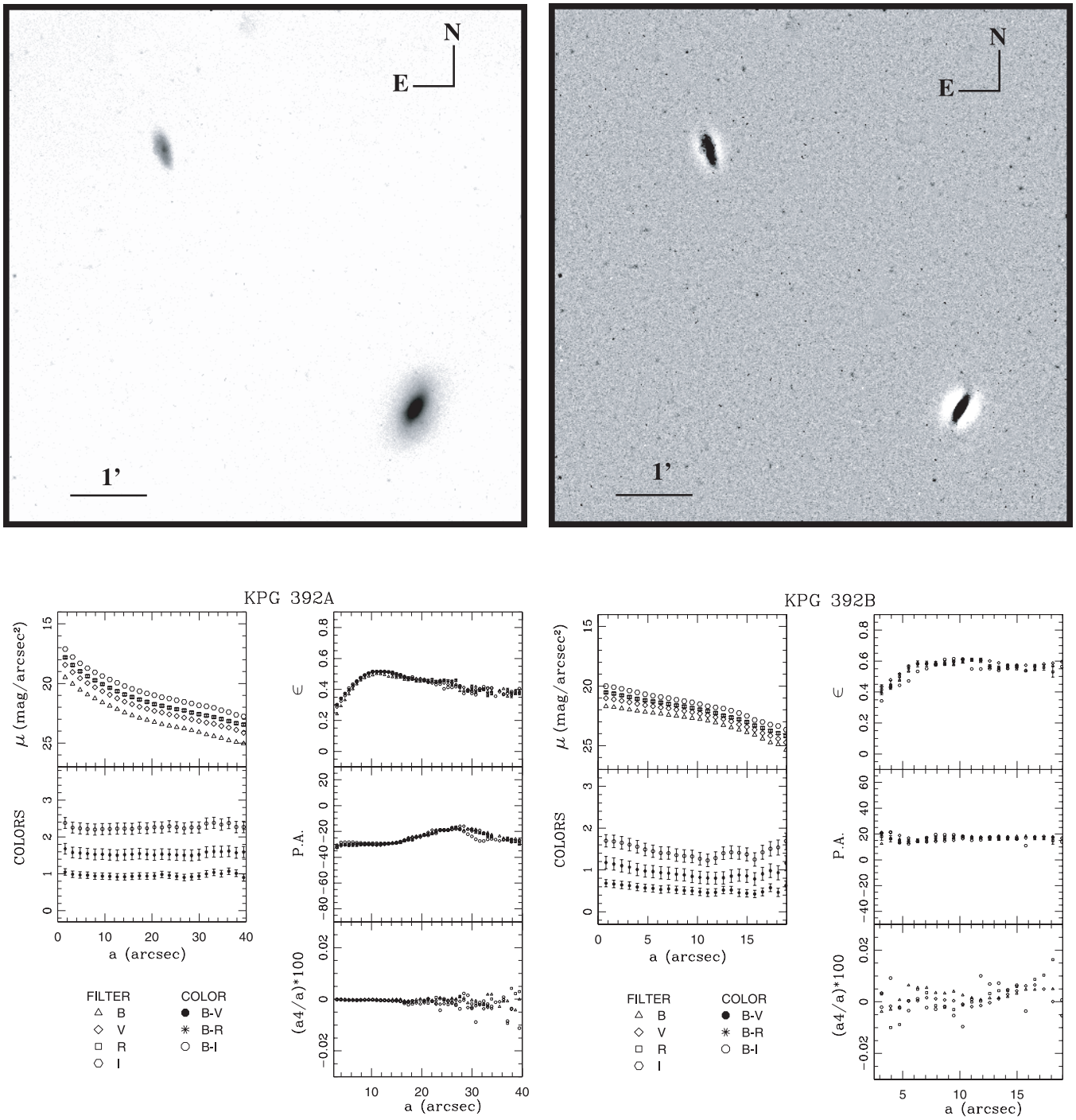

Fig. 8. KPG392 Mosaic. *Top left*: *B*-band image. *Top right*: *B*-band filtered image. *Bottom left*: surface brightness profile and geometric parameters for KPG392A. *Bottom right*: surface brightness profile and geometric parameters for KPG392B.

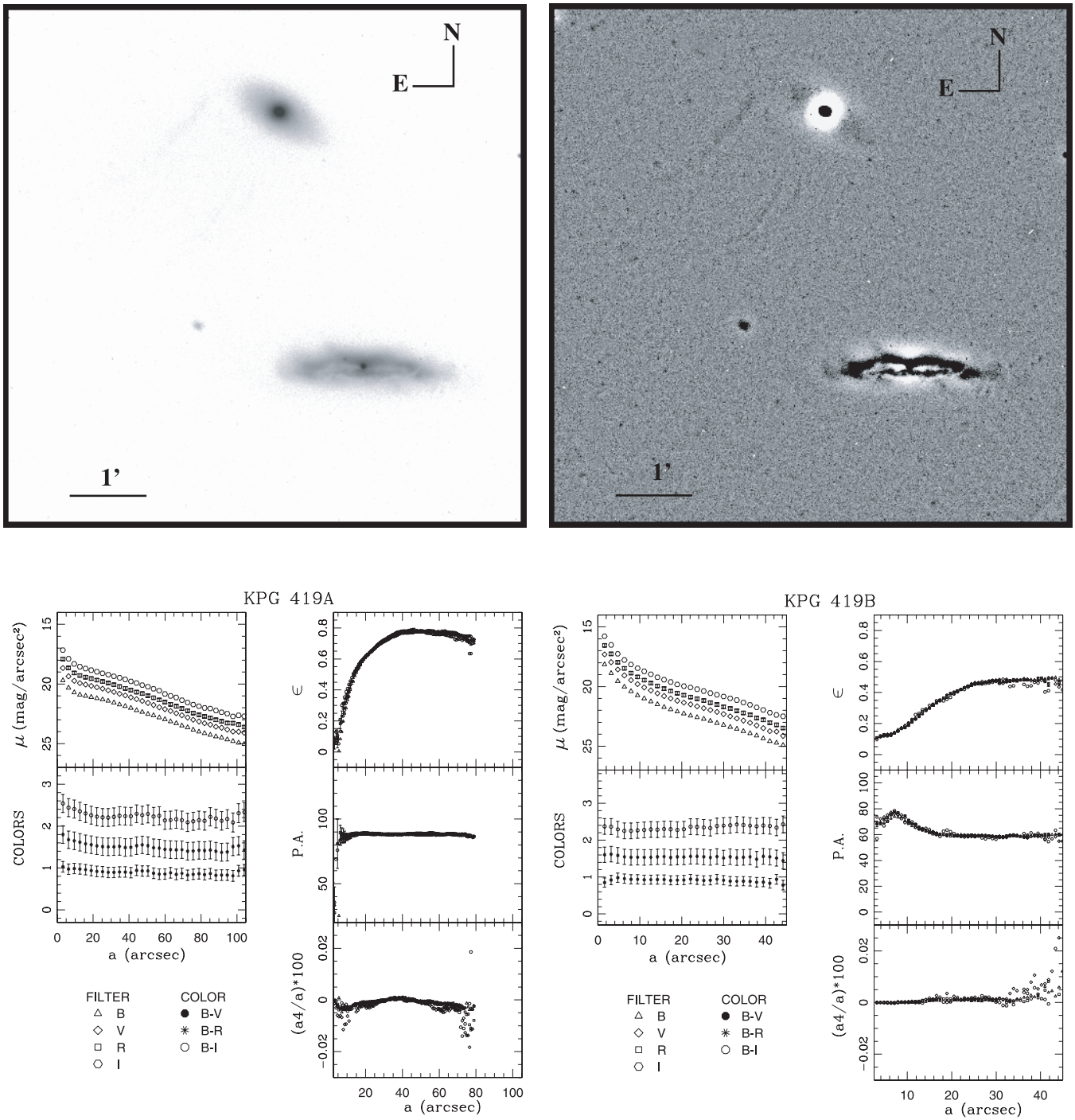

Fig. 9. KPG419 Mosaic. *Top left*: *B*-band image. *Top right*: *B*-band filtered image. *Bottom left*: surface brightness profile and geometric parameters for KPG419A. *Bottom right*: surface brightness profile and geometric parameters for KPG419B.

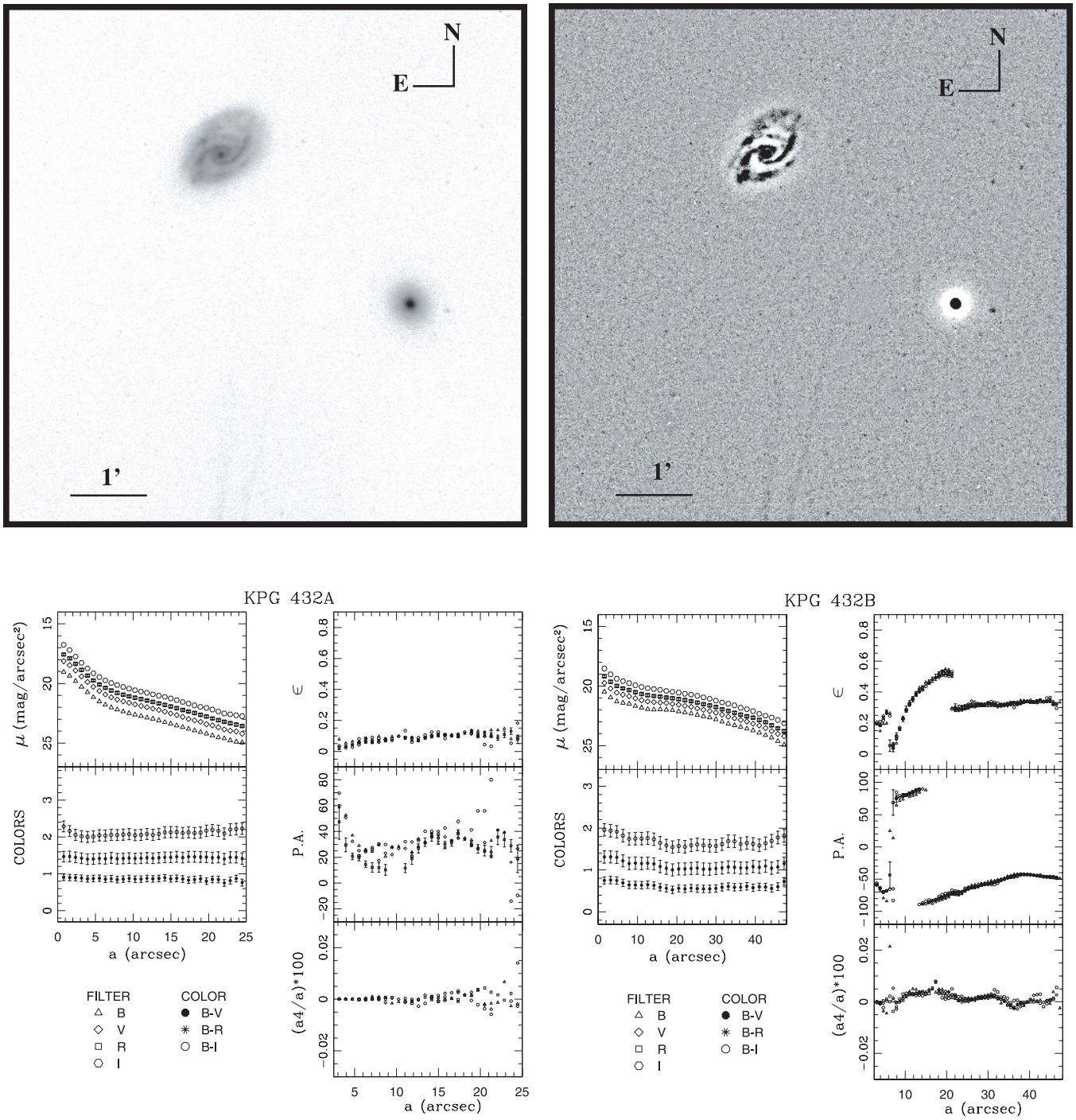

Fig. 10. KPG432 Mosaic. *Top left*: *B*-band image. *Top right*: *B*-band filtered image. *Bottom left*: surface brightness profile and geometric parameters for KPG432A. *Bottom right*: surface brightness profile and geometric parameters for KPG432B.

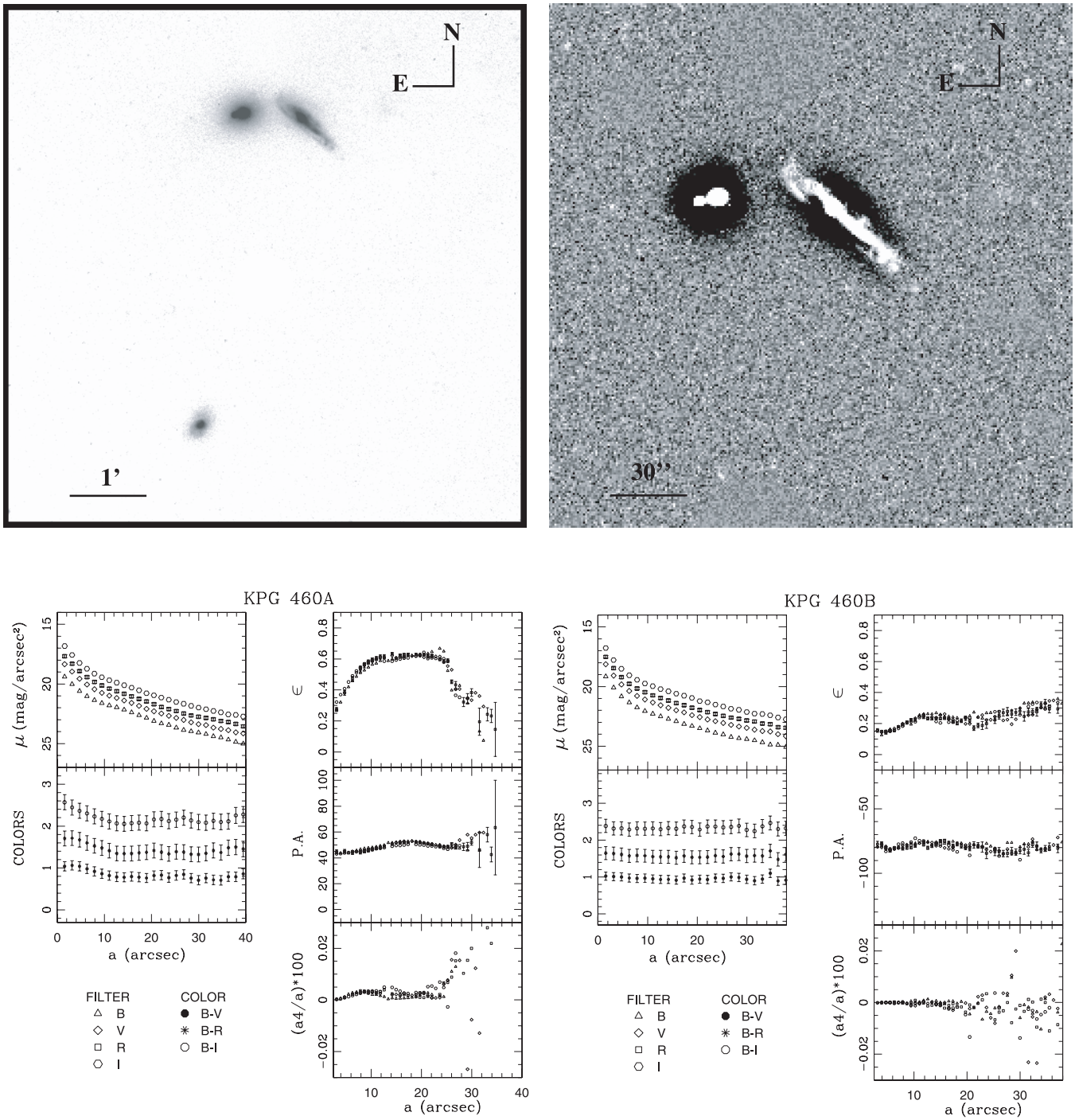

Fig. 11. KPG460 Mosaic. *Top left*: *B*-band image. *Top right*: *B*-band filtered image. *Bottom left*: surface brightness profile and geometric parameters for KPG460A. *Bottom right*: surface brightness profile and geometric parameters for KPG460B.

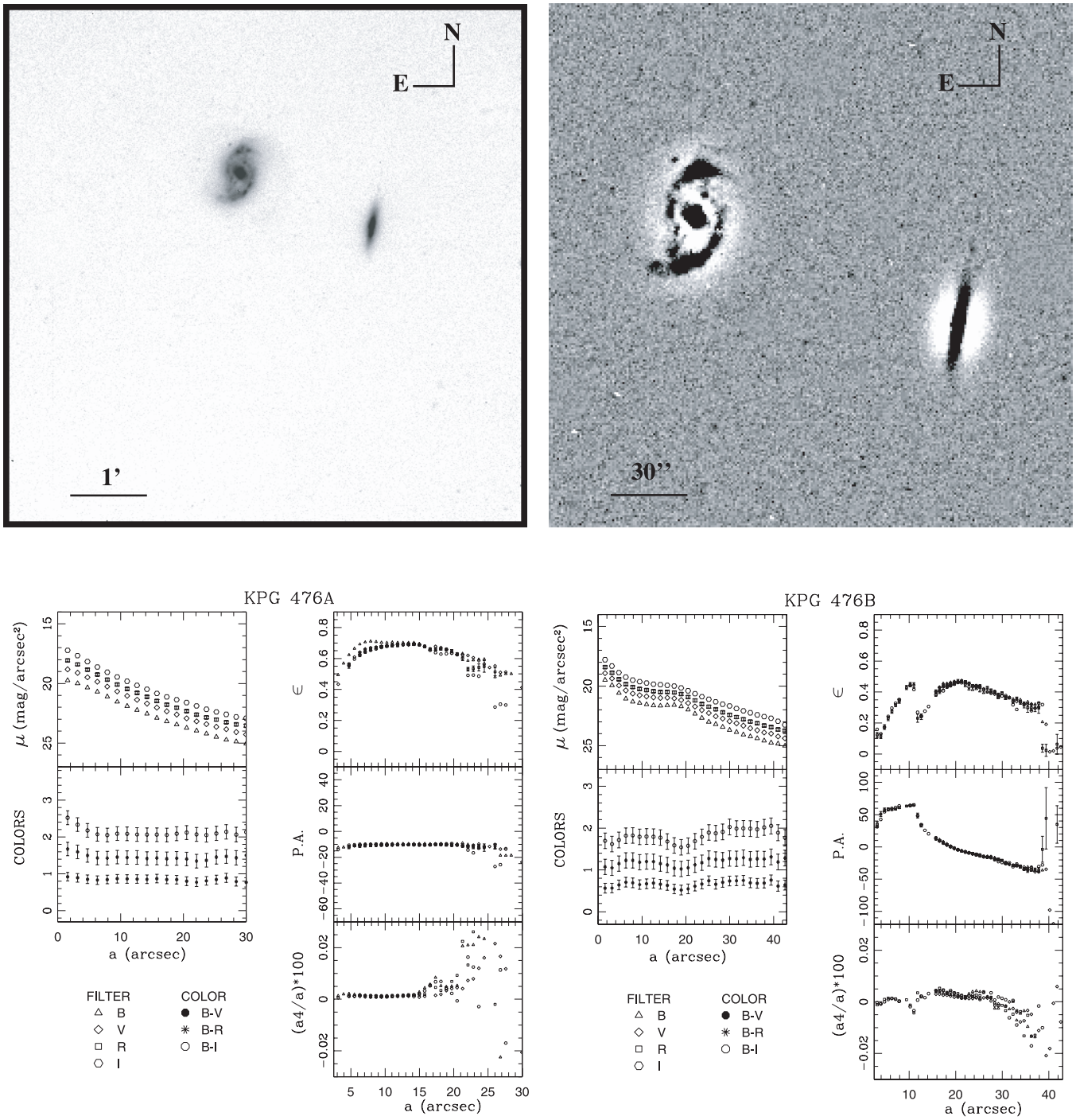

Fig. 12. KPG476 Mosaic. *Top left*: *B*-band image. *Top right*: *B*-band filtered image. *Bottom left*: surface brightness profile and geometric parameters for KPG476A. *Bottom right*: surface brightness profile and geometric parameters for KPG476B.